PCCP

Cite this: *Phys. Chem. Chem. Phys.*, 2011, **13**, 9397–9406

www.rsc.org/pccp

PAPER

The structure of glycerol in the liquid state: a neutron diffraction study

J. J. Towey,[a] A. K. Soper[b] and L. Dougan*[a]

Received 12th October 2010, Accepted 3rd March 2011
DOI: 10.1039/c0cp02136a

Neutron diffraction coupled with hydrogen/deuterium isotopic substitution has been used to investigate the structure of the pure cryoprotectant glycerol in the liquid state at 298 K and 1 atm. The neutron diffraction data were used to constrain a 3 dimensional computational model that is experimentally relevant using the empirical potential structure refinement (EPSR) technique. These simulations lead to a model structure of the glycerol molecule that is consistent with the experimental data. Interestingly, from interrogation of this structure, it is found that the number of hydrogen bonds per molecule is larger than had previously been suggested. Furthermore, converse to previous work, no evidence for intra-molecular hydrogen bonds is found. These results highlight the importance and relevance of using experimental data to inform computational modelling of even simple liquid systems.

Introduction

Glycerol ($CH_2OHCHOHCH_2OH$) has been the subject of considerable and long-standing scientific interest. This attention is partly due to glycerol's ability as a glass former and the nature of its glass transition has been the subject of many investigations.[1,2] Glycerol is active in maintaining the structure of biological macromolecules and is thought to promote self-assembly through preferential hydration.[3,4] Interest in glycerol has also stemmed from its extensive use in nature as a cryoprotectant, where cells or whole tissues are preserved under cooling to sub-zero temperatures. In nature, a diverse range of organisms, including bacteria, yeast, desert plants, insects, fish and reptiles, utilise cryopreservation as a vital tool for survival in adverse environmental conditions.[5] In these organisms glycerol is used in high concentrations as a colligate cryoprotectant that is thought to raise the osmolarity of body fluids and reduce the water available to form extracellular ice.[6] The discovery of the cryoprotective properties of glycerol by Polge *et al.* in 1949 led to the development of artificial cryopreservation.[7] This early success led many investigators to attempt the preservation of other cells and tissues by similar empirical procedures. Indeed, the literature of the 1950–1960s is dominated by efforts to achieve cryopreservation in a variety of cell types through empirical variations of freezing rates, thawing rates and cryoprotectant concentrations.[8] In the present day, cryoprotectants like glycerol are widely used as components for storage of biological and pharmaceutical products at low temperature.

To understand how glycerol functions as a glass former and cryoprotectant, the physical properties of glycerol and its mixtures with water have been studied extensively using a number of methods including molecular dynamics,[9] thermodynamic measurements,[10] NMR,[11] infrared,[12] and Raman spectroscopy.[11,13] While these studies have provided useful insights for understanding the dynamic behaviour of glycerol, the manner in which glycerol hydrogen bonds is yet to be elucidated. Indeed, a correspondingly thorough understanding of the structure of glycerol, at the molecular level, could help to explain the behaviour of a broad family of other glass formers. Such structural insight into a cryoprotectant system could also provide clues to the physical mechanism of cryopreservation.

Glycerol is a sugar alcohol with three hydroxyl groups that are thought to be responsible for its high solubility in water. Liquid glycerol exhibits an anomalous temperature behaviour of the viscosity coefficient[14,15] and of dielectric relaxation times,[16,17] thought to be due to the existence of an extended hydrogen-bond network.[18] On account of molecular flexibility, asymmetry and ability to form hydrogen bonds, glycerol is an intricate substance to study at the molecular level. Indeed, the conformational space of glycerol is complex, with six types of conformer existing, classified in the literature on the subject according to the dihedral angles involving the two CCCO torsions.[19] For that reason computational modelling using an acceptable molecular model for glycerol is a highly desirable prospect. Root and Stillinger have studied glycerol by molecular dynamics simulation (32 molecules), focusing on the structure of the liquid and amorphous solid.[20] A later study by Root and Berne has reported on molecular dynamics investigations of hydrogen bonding in liquid glycerol and the effects of pressure on the hydrogen bond network.[21] More recently Chelli *et al.* have completed molecular dynamics and density

[a] *School of Physics and Astronomy, University of Leeds, Leeds, LS2 9JT, UK. E-mail: L.Dougan@leeds.ac.uk*
[b] *ISIS Facility, Rutherford Appleton Laboratory, Chilton, Didcot, Oxon, OX11 OQX, UK*

Table 1 Glycerol samples for which the structure factor has been measured with neutron diffraction on the SANDALS instrument. Glycerol (99.5%), glycerol-*d*3 (98 atom% D), glycerol-*d*8 (98 atom% D) were supplied by Sigma-Aldrich

Sample No.	Sample Name	Description
1	Glycerol-D8	Fully deuterated (98 atom% D)
2	Glycerol-D5	Carbonyl atoms are deuterium and hydroxyl are hydrogen (98 atom% D),
3	Glycerol-D8/D5	1 : 1 mixture of samples 1 and 2
4	Glycerol-H8	Fully protiated (99.5%),
5	Glycerol-H8/Glycerol-D8	1 : 1 mixture of samples 1 and 4

functional theory based studies of the condensed phases of glycerol, analysed in relation to the backbone conformation of the molecule.[22–24] Remarkably, there are few experimental structural studies of pure glycerol, the most recent being an X-ray diffraction study of the hydrogen bonding nature of glycerol.[27] An earlier neutron diffraction study of the fully deuterated compound was completed by Champeney and Dore.[25,26] X-ray diffraction has also been used to study the hydrogen bonding nature of glycerol.[27] However, the conclusions that could be drawn from these early experimental studies are limited due to inability to separate the signals from different atoms unambiguously.

The lack of experimental data and the variability of results produced using computer simulations mean that a full systematic experimental investigation of the structure of glycerol is required. In the present study we use experimental and computational methods to allow for the determination of a complete set of partial radial distribution functions on glycerol in the liquid state. Neutron diffraction is a suitable probe for the structural study of liquid glycerol due to the large scattering cross section of deuterium and the high contrast achievable using H/D selective substitution on specific hydrogen sites in the molecule. The main goal of this work was to obtain high quality structural data of liquid glycerol at 298 K that can allow determination of the conformation of the molecule and investigation of the hydrogen bonding interactions between glycerol molecules. This information is important for evaluating the length scales and magnitude of intra- and inter-molecular hydrogen bonds in the system. The availability of new and detailed experimental structural information will provide a fundamental benchmark for spectroscopic and computational studies aimed at characterising the properties of systems involving glycerol. This has been accomplished by supplementing the isotopic substitution neutron diffraction experiments with computer modelling. Specifically, the modelling is a three-dimensional molecular reconstruction using the Empirical Potential Structure Refinement (EPSR) method which is constrained by experimental neutron diffraction data, described in the following section.

Experimental methods

A. Neutron diffraction experiments

Neutron diffraction coupled with isotopic substitution allows labelling of individual atomic sites in a molecule and the extraction of selected pair radial distribution functions (RDFs), $g(r)$. Neutron diffraction measurements were completed on the SANDALS time-of-flight diffractometer at the ISIS pulsed neutron facility at the Rutherford Appleton Laboratory, UK. SANDALS is a total scattering neutron diffractometer optimised for the study of liquids and amorphous samples containing light elements. The physical quantity measured by the diffractometer is the differential scattering cross section $d\sigma/d\Omega$ as a function of the exchanged wave vector Q (defined as the difference between the incident and the scattered neutron wave vectors). Through the theory[28] of neutron scattering, it is possible to relate this quantity to the static structure factor $S(Q)$, which is the Fourier transform of the atomic pair distribution function $g(r)$.[29] The function $g(r)$ shows how atomic densities vary as a function of radial distance, r, from any particular atom.

Protiated and deuteriated samples of anhydrous glycerol were obtained from Sigma-Aldrich and used without additional purification. Specifically, the protiated glycerol sample was molecular biology grade ($\geq$ 99.5% purity), deuterated glycerol (98% purity) and partially deuterated glycerol where the carbonyl atoms are deuterium while the hydroxyl are hydrogen (98%). A Karl-Fischer titration of a sample of glycerol treated the same way as the diffraction samples revealed a water content at the level of parts per million, which was similar to the quoted purity from the supplier. Water content at this low level would not be detectable in the neutron experiment. A total of 5 isotopically distinct samples were measured and are shown in Table 1. The samples were loaded directly into the sample container which is made of a titanium zirconium alloy and is a flat plate of internal dimensions 1 mm by 35 mm by 35 mm with a wall thickness of 1.1 mm and which gives negligible coherent scattering signal. The sample container was held in a custom-built loading platform which securely holds the container. Glycerol samples were deposited in the sample container using sterile syringes, after which the sample container was securely sealed using a deformable plastic seal and mounting screws. After the sample container had been sealed they were placed in a vacuum oven. Sample cans were weighed before and after placement in a vacuum oven to ensure the container is sealed and no evaporation had occurred. These cells were mounted on an automated sample changer to cycle through the samples. The differential scattering cross-section for each sample was obtained by normalising to a vanadium standard. Corrections for attenuation and multiple scattering were made using the ATLAS program suite which has been detailed previously.[30] A further correction for inelastic scattering was made and has been described in detail elsewhere.[31] Neutron diffraction on solutions yields the quantity, F(Q), which is the total interference differential scattering cross section, and which is the sum of all partial structure factors $S_{\alpha\beta}$ (Q) present in the sample each weighted by their composition c and scattering intensity b, $F(Q) = \Sigma_{\alpha\beta} c_\alpha c_\beta b_\alpha b_\beta (S_{\alpha\beta}(Q) - 1)$, where Q is the magnitude of the change in

momentum vector by the scattered neutrons ($Q = (4\pi//\lambda)\sin\theta$). Fourier transform of $S_{\alpha\beta}(Q)$ gives the respective atom-atom radial distribution functions (RDFs) $g_{\alpha\beta}(r)$, and integration of $g_{\alpha\beta}(r)$, gives the coordination numbers of atoms α around atoms β between two distances r_1 and r_2.

B. Computational modelling

In this paper we refer to 6 distinct atomic components in glycerol molecules (see Fig. 1). The carbon atoms are labelled CC and CG and refer to the central and distal carbon atoms respectively. The oxygen atoms are labelled OC and O corresponding to the oxygen atoms attached to the central and distal carbon atoms respectively. The hydrogen atoms are labelled H and HG for the hydroxyl and methyl hydrogen atoms respectively. A full structural characterisation of the system therefore requires the determination of 21 site-site radial distribution functions, which is well beyond the possibility of any existing diffraction technique by itself.

Thus, to build a model of glycerol liquid structure, these experimental data are used to constrain a computer simulation. However, unlike conventional simulations, such as molecular dynamics or *ab intio* calculations which use a fixed intermolecular potential, part of the potential used here is obtained directly from the diffraction data. This potential drives the structure of the three-dimensional model toward molecular configurations that are consistent with the measured neutron diffraction data. This process is called Empirical Potential Structure Refinement (EPSR).[32] EPSR aims to produce a model with a simulated differential scattering cross section which fits the experiment results as closely as possible. Given that in this case there are more site-site radial distribution functions than diffraction data sets, extra information is required to define the structure. This is achieved by forcing the glycerol molecules in the simulation box to adopt the expected molecular geometries. A reference interaction potential is also used which serves to generate hydrogen bonding between the relevant atom sites and to prevent atomic overlap at unrealistic distance ranges. The combined empirical and reference potentials do not guarantee the final reconstruction of the structure is exactly correct, but they do ensure it is consistent with the diffraction data as well as being physically plausible.

For the simulations, a total of 1000 glycerol molecules were contained in a cubic box of the appropriate dimension to give the measured density at 298 K. The intra-molecular structure was optimised using the computational chemistry software Ghemical 2.98.[39] This resulted in an $\alpha\alpha$ dihedral angle conformation structure, defined in the next section. A three-dimensional computer model of the solution is constructed and equilibrated using relevant interaction potentials (see Fig. 1 for molecule conformation and Table 2 and 3 for atomic geometry). The charges and Lennard-Jones constants are shown in Table 4. Periodic boundary conditions were imposed and the Coulomb interactions were truncated by means of a derivative of the reaction field method,[33] and other interactions were truncated as described previously,[34] using a radial cut-off of 12 Å in all cases.

Information from the diffraction data is then introduced as a constraint whereby the difference between observed and calculated interference differential scattering cross section enters as a perturbation potential to drive the computer model (*via* Monte Carlo updates of atomic positions) towards agreement with the measured data. The perturbation is refined in successive iterations of the procedure until a satisfactory fit is obtained. In this way an ensemble of three-dimensional molecular configurations of the mixture is generated which exhibit average structural correlations that are consistent with the diffraction data.

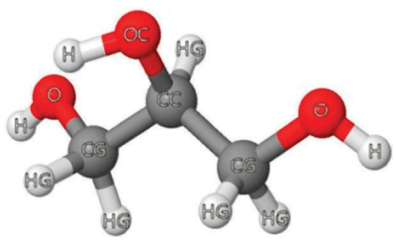

Fig. 1 The glycerol molecule. Single atoms have been labelled according to the symbols used in the simulation and throughout this paper where the carbon atoms are labelled CG and CC, the oxygen atoms O and OC, the hydroxyl hydrogen atoms, H and the methyl hydrogen atoms, HG.

Results and discussion

Glycerol molecule conformer determination

In the glycerol molecule all bonds between atoms are single and there is therefore considerable rotational freedom. The traditional classification of the molecular structure of this molecule is based on the concept of backbone conformation, defined by the structure of the heavy atoms (carbon and oxygen) irrespective of the position of the hydrogen atoms. These backbone conformations are defined in terms of the dihedral angles which are formed at the intersection between 2 specified planes within the molecule.[19] Fig. 2a illustrates how 2 planes can be set-up within the molecule and how the dihedral angle is then defined. Each glycerol molecule is assigned two dihedral angles, φ_1 and φ_2, which are formed by the three carbon atoms and the two terminal oxygen atoms (O). Specifically, each terminal CH_2OH group can rotate about the other backbone carbon-carbon bond. For glycerol the two planes are defined by the bond distances between intra-molecular bonded atoms O–CG–CC and CG–CC–CG, yielding one dihedral angle φ_1. This dihedral angle can be defined by 3 regions known as α, β and γ,[19] where

Table 2 Geometry for intra-molecular bonds in glycerol molecules used in the EPSR simulations. The geometry has been optimised using the computational chemistry software Ghemical 2.98[39]

Intra-molecular Bond	Length (Å)
O–CG	1.45
O–H	0.97
OC–H	0.97
OC–CC	1.45
CG–CC	1.54
CG–HG	1.08
CC–HG	1.08

Table 3 Geometry for intra-molecular angles in glycerol molecules used in the EPSR simulations. The geometry has been optimised using the computational chemistry software Ghemical 2.98[39]

Intra-molecular Bond	Angle (°)
CG–O–H	109.90
CC–OC–H	108.33
O–CG–CC	108.88
CC–CG–HG	110.17
O–CG–HG	109.51
HG–CG–HG	108.57
CG–CC–CG	111.20
OC–CC–CG	108.72
CG–CC–HG	109.61
OC–CC–HG	108.96

Table 4 Lennard-Jones parameters, masses and Coulomb charges defining the potentials used for EPSR simulations of glycerol at 298 K

Atom Name	ε (kJ mol^{-1})	σ(Å)	m (a.m.u.)	q (e)
OC	0.65	3.1	16	−0.624
O	0.65	3.1	16	−0.624
CG	0.80	3.7	12	0.107
CC	0.80	3.7	12	0.170
H	0	0	2	0.392
HG	0	0	2	0.063

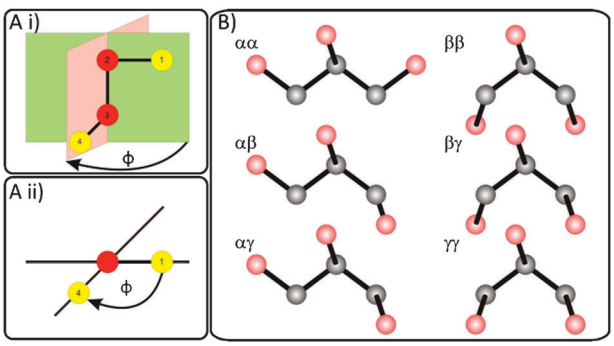

Fig. 2 Ai: Diagram of a simple 4 atom molecule with the 2 planes that can be constructed using the 3 bonds to produce pairs of vectors ($\bar{1}\bar{2}$ $\bar{2}\bar{3}$ and $\bar{2}\bar{3}$ $\bar{3}\bar{4}$). Aii: when the molecule is rotated to view it along the $\bar{2}\bar{3}$ vector the dihedral angle can be measured as the angle between $\bar{1}\bar{2}$ and $\bar{3}\bar{4}$ in a clockwise direction. Two dihedral angles are measured within each glycerol molecule using the 3 carbon atoms and either "end" oxygen (O–CG–CC–CG and CG–CC–CG–O). These angles are split in to 3 regions known as α ($120° \leq \varphi \leq 240°$), β ($240° < \varphi \leq 360°$) and γ ($0° < \varphi < 120°$). Therefore, with these 2 measurements of φ, each glycerol conformation can be described using the appropriate expression of 2 Greek letters (*e.g.* αα). B: A schematic diagram of the six conformers that can be produced using the nomenclature of Bastiensen.[19] Here, the oxygen atoms are red and the carbon atoms are black. The hydrogen atoms have been removed to aid clarity.

$$\alpha = 120° < \varphi < 240° \quad (1)$$

$$\beta = 240° < \varphi < 360° \quad (2)$$

$$\gamma = 0° < \varphi < 120° \quad (3)$$

As there are two terminal oxygen atoms in glycerol we define the bond distances between two further planes CC–CG–O and CG–CC–CG and measure a second dihedral angle φ_2. Therefore each glycerol molecule conformer can be defined in terms of two dihedral angles, φ_1 and φ_2 which are assigned either α, β or γ, resulting in six possible backbone conformers, αα, αβ, αγ, ββ, βγ and γγ. Here heterogeneous pairs, such as αβ and βα, are not counted as separate conformers as they are indistinguishable using this nomenclature. A schematic representation of the 6 conformers of glycerol are shown in Fig. 2b.

The conformational structure of glycerol in the crystalline state has been identified by X-ray diffraction which revealed the presence of only αα backbone conformers.[35] For all other phases, the available experimental and theoretical data are contradictory. In particular, for the liquid and glassy state, available experimental studies have been unable to ascertain the conformational distribution of glycerol conformers. In two neutron diffraction studies the αα and αγ conformations were invoked to explain the observed structure factors.[25,26] On the other hand, in a recent neutron scattering investigation, the observed structure factors of glassy glycerol (180 K) were fit assuming βγ backbone conformers.[36]

In order to shed light on the structural properties of glycerol in the liquid state we have completed a systematic study of glycerol conformations using EPSR combined with neutron diffraction experimental data. For a full understanding of glycerol in the liquid state it is important to determine which conformer/mixture of conformers produces the best fit to the experimental data presented here.

To this end a series of EPSR simulations were completed for different conformations of the glycerol molecule. Each simulation was then compared to the experimental data to determine which conformation/mixture of conformations of glycerol best described the data. In all 7 different conformational arrangements of glycerol were tested. These included the six possible backbone conformers as defined above; αα, αβ, αγ, ββ, βγ and γγ, and a model where all dihedral angles were free to rotate to all angles.

EPSR allows the molecules to have a degree of rotational freedom and these can be restricted by specifying bond distances between the end members of each dihedral angle definition (O and CG in this case). A single distance however does not uniquely constrain the dihedral angle, so in order to constrain two planes and thus two dihedral angles, φ_1 and φ_2 two additional bond distances were specified requiring two further dihedral angles to be described, namely φ_3 and φ_4. These bond distances and angles were defined using the two planes O–CG–CC and CG–CC–OC for φ_3 and CC–CG–O and OC–CC–CG for φ_4. In each case the starting potential, bond lengths and angles for the EPSR simulations were the same (Table 2 and 4) and only the dihedral angles were modified (Table 5) to meet the angular requirements of each conformer.[19]

The use of four bond distances and thus four dihedral angles to describe glycerol does not ensure that all molecules are of the desired conformation. This is due to the level of disorder of the bond angles required to accurately describe a liquid sample. The models are, therefore, comprised, after equilibration, of a mixture of conformers with ~70–85% of the desired molecule structure. Table 6 shows the final distribution of conformers within each model after equilibration.

For each system a comparison between the interference differential cross sections obtained from the ensemble-averaged

Table 5 Geometry for intra-molecular dihedral angles in the different conformations of glycerol molecules used in the EPSR simulations (see text for definition of each of the conformations). Here φ_1 and φ_2 refer to each of the O–CG–CC–CG dihedral angles and φ_3 and φ_4 refer to each of the O–CG–CC–OC dihedral angles. A further simulation was completed without any dihedral angle constraints and is called "No dihedrals"

Model	φ_1 (°)	φ_2 (°)	φ_3 (°)	φ_4 (°)
αα	180	180	60	−60
αβ	180	60	60	180
αγ	180	−60	60	60
ββ	−60	60	180	180
βγ	−60	−60	180	60
γγ	60	−60	60	−60

Table 6 Percentage distribution of conformations present in each EPSR simulation after equilibration (see text for definition)

Model	αα	αβ	αγ	ββ	βγ	γγ
αα	85.7	0.0	12.1	0.0	0.0	2.2
αβ	0.0	83.5	10.4	0.0	4.3	1.8
αγ	6.5	7.1	82.2	0.0	0.1	4.1
ββ	0.0	0.0	0.0	69.4	30.2	0.4
βγ	0.0	7.8	1.1	7.4	80.5	3.2
γγ	0.7	1.1	10.4	0.4	7.9	79.5
No dihedrals	37	23.4	18.5	5.6	5.6	9.9

EPSR D(Q) and the experimentally measured data F(Q) was made. The quality of fit of $D_i(Q)$ to $F_i(Q)$ was determined using a parameter known as the *R*-factor which is an un-weighted sum defined as,

$$R = \frac{1}{M}\sum_i \frac{1}{n_Q(i)}\sum_Q [D_i(Q) - F_i(Q)]^2 \qquad (4)$$

where M is the number of datasets, $D_i(Q)$ is the simulated structure factor, $F_i(Q)$ is the simulated differential cross section for the ith dataset and $n_Q(i)$ is the number of Q values within the ith dataset. An *R*-factor close to zero then denotes a good fit.

Table 7 shows the *R*-factors measured for each of the 7 EPSR simulations. It can be seen that the *R*-factor is lowest for EPSR simulations having the αβ conformation. Interestingly, the EPSR simulation in which dihedral angles are free to rotate gives an *R*-factor which lies within the mid range of *R*-factor values (Table 7). The quality of fit of all seven EPSR simulations can be compared visually by plotting the sum of the residuals squared ($\Sigma[D_i(Q)–F_i(Q)]^2$) over all datasets as a function of Q (Fig. 3). The plots are ordered from the smallest (bottom) to

Table 7 Quality of fit (*R*-factor) of the ensemble-averaged EPSR D(Q) and the experimentally measured data F(Q) for the 7 different EPSR simulations

Model	*R*-factor
αβ	0.1734
αγ	0.1931
αα	0.1986
ββ	0.2090
No Dihedrals specified	0.2233
βγ	0.2448
γγ	0.3429

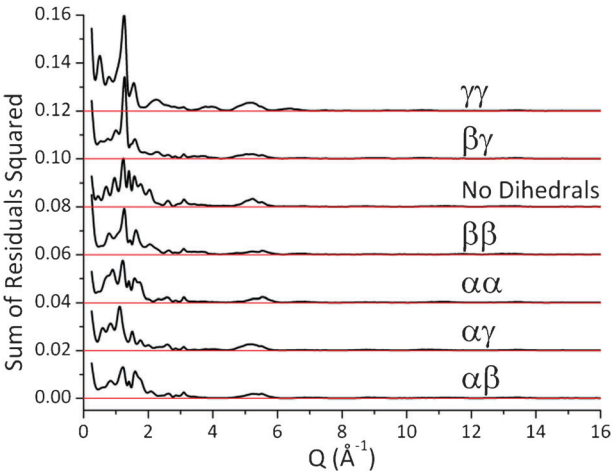

Fig. 3 The sum of residuals squared ($\Sigma[D(Q)–F(Q)]^2$) as a function of Q for the 7 EPSR simulations. Here, the residual is the difference between the measured structure factor, F(Q), and the simulated values, D(Q). The 7 models have been arranged in order of increasing *R*-factors with the best fit, αβ, at the bottom. This shows that the αβ model produces the closest fit to the experimental data.

largest (top) *R*-factors. This shows that the αβ EPSR simulation provides the closest fit to the measured data.

The simulated and measured structure factors for the αβ EPSR simulation can be compared in Fig. 4. Here the $D_i(Q)$ obtained from the EPSR simulation (red lines) are compared to the neutron diffraction data $F_i(Q)$ (black circles) for glycerol at 298 K. In Fig. 4 the $F_i(Q)$ have been labelled using the system shown in Table 1 and have been shifted vertically for clarity. Discrepancies are observed in the low Q region and are caused by difficulties in removing the effect of nuclear recoil from the measured data. However, this recoil effect is expected to have a monotonic dependence on Q and so does not influence the model structure to any significant extent.

From this analysis it can be concluded that the EPSR simulation with the majority of the molecules in the αβ

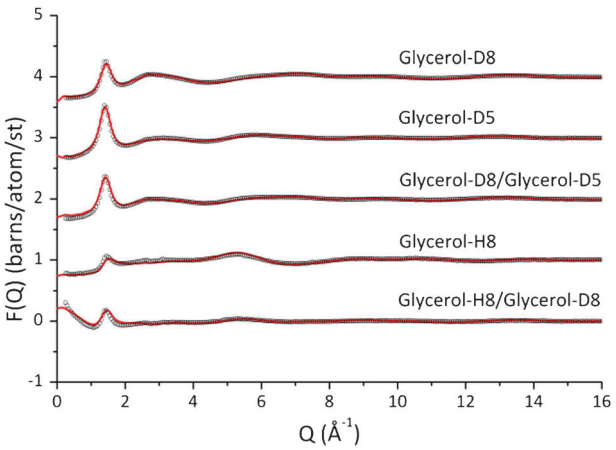

Fig. 4 Fits (red lines) obtained by the EPSR analysis using the αβ model (Table 5 and 7) compared to the original data (black circles) for glycerol at 298 K. The data and fits are labelled according to Table 1 and have been shifted vertically for improved clarity. The data shown here confirm that the αβ model produces a simulation that is in good agreement with the experimental data.

conformation produced a final reconstruction of the structure of glycerol that is consistent with the diffraction data as well as being physically plausible. This result differs from previous neutron diffraction studies where the αα and αγ glycerol conformations were invoked to explain the observed structure factors.[25,26] Previously, an extensive molecular dynamics study of the conformational structure of glycerol examined the conformational distribution of the molecule in the condensed phases.[23,24] This study found that in the liquid state (300 K) 48% of conformers were αα and 46% were αγ. A recent density functional theory based simulation examined glycerol conformations and compared them to experimental infrared spectra of the gas and liquid state.[22] This study found that αα conformations predominate (70%) with a significant proportion of αγ conformations (27%). Again, these results differ from the probability distribution of conformers found in the present study (Table 6).

It is interesting to consider whether the conformations of glycerol found in the liquid state are stabilised by the inter-molecular interactions between molecules or if their relative probability is controlled by the intra-molecular interactions. In the present study, while the optimised intra-molecular structure of the glycerol molecule yielded an αα conformation, the conformational distribution of glycerol in the liquid state was quite different. As noted above, the EPSR simulation which gave the best agreement with the experimental data had ~84% glycerol molecules in the αβ conformation, 10.4% in the αγ conformation, 4.3% in the βγ conformation and 1.8% in the γγ conformation. This suggests that inter-molecular bonding is important in determining the conformation of glycerol molecules in the liquid state. This is in disagreement with work by Chelli who found that inter-molecular hydrogen bonds did not significantly stabilise energetically unfavoured conformers.[23]

It is appropriate here to speculate briefly why the present results do not show full agreement with previous results. As regards the previous neutron diffraction work,[25,26] in those cases the molecular conformation was obtained by fitting a single molecule form factor to the diffraction data. Such a procedure ignores the likely variability of conformation from one molecule to the next in a condensed liquid such as this one, and also ignores the fact that inter-molecular and intra-molecular distances often overlap in this system, so that fitting a single intra-molecular form factor which largely ignores the pronounced *inter*-molecular correlations is prone to give inaccurate results. It is less clear why the present results disagree with the earlier MD results, although one could draw attention to the fact that the different MD simulations do not agree with each other, so a discrepancy between the present simulations and earlier ones is not unexpected. The present simulations start from the αα conformation, but obtaining the best fits requires a high preponderance of αβ conformations. The changes in *R*-factor between the various conformations are not huge, but appear to be significant. This is borne out by visual inspection of Fig. 3, where the αβ conformation clearly has the smallest residual. Nonetheless one should always be aware when interpreting diffraction data of this kind, using a computer simulation model which has only pairwise additive forces, that another solution to the structure is possible, *e.g.* one which might involve three- or many-body forces. Unfortunately techniques to discover the influence of such forces are very limited at the present time.

Glycerol hydrogen bonding

In order to understand more about the structure of glycerol in the liquid state the EPSR simulation of the αβ conformation system was analysed further (Table 6). To understand the structure of glycerol it is important to investigate the nature of the bonds that are present. Given glycerol's ability to hydrogen bond we examined both the intra- and inter-molecular radial distribution functions (RDFs) to gain an understanding of both the number and types of bonds that are present.

Intra-molecular hydrogen bonding

The intra-molecular RDFs for oxygen-oxygen ($g_{O–OC}(r)$ and $g_{O–O}(r)$) and oxygen-hydroxyl hydrogen ($g_{O–H}(r)$ and $g_{OC–H}(r)$) pairings are shown in Fig. 5. Clear peaks can be seen within the $g_{O–OC}(r)$ function at ~2.8 Å and ~3.7 Å. The peak within $g_{O–O}(r)$ can be found at ~4.3 Å. The peak at ~2.8 Å in the $g_{O–OC}(r)$ function is of particular interest as this is indicative of hydrogen bonding. For this to be classified as a hydrogen bond it is necessary to have a hydrogen atom at some point between the two oxygen atoms. This would be shown by a peak within either $g_{O–H}(r)$ or $g_{OC–H}(r)$ that could be ascribed to a non-covalent bond. The oxygen-hydrogen covalent bond length is 1.0 Å. We would therefore expect to observe a peak at ~1.8 Å in the $g_{O–H}(r)$ or $g_{OC–H}(r)$. From Fig. 5b a peak is observed at ~1.0 Å corresponding to

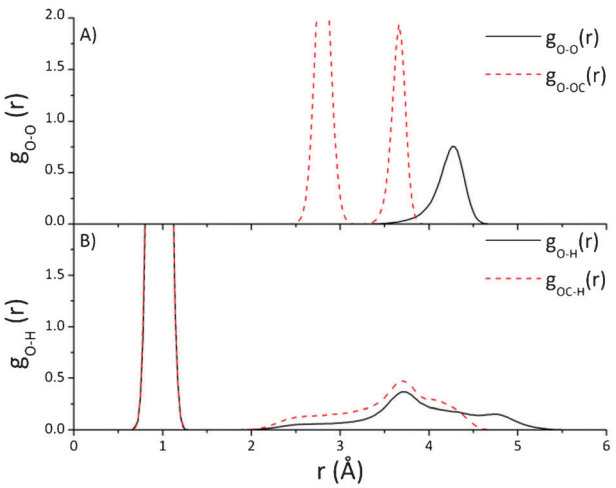

Fig. 5 Intra-molecular partial radial distribution functions (RDFs) for oxygen-oxygen ($g_{O–OC}(r)$ and $g_{O–O}(r)$) and oxygen-hydroxyl hydrogen ($g_{O–H}(r)$ and $g_{OC–H}(r)$) pairings taken from neutron diffraction data and the EPSR simulation of glycerol at 298 K. In the oxygen-oxygen RDFs (A) two clear peaks can be seen within the $g_{O–OC}(r)$ function at ~2.8 Å and ~3.7 Å. A prominent peak can be seen at ~4.3 Å within the $g_{O–O}(r)$ function. The peak at ~2.8 Å is of particular interest as this is indicative of hydrogen bonding. In the oxygen-hydrogen RDFs (B) the peak due to covalently bonded hydrogen can be seen at ~1.0 Å in $g_{O–H}(r)$ and $g_{OC–H}(r)$. A peak would be expected at ~1.8 Å if there were intra-molecular hydrogen bonds within glycerol. A prominent peak is not present in $g_{O–H}(r)$ and $g_{OC–H}(r)$ and therefore there is little evidence for intra-molecular hydrogen bonding.

covalently bonded hydrogen. However, no peak is observed at ~1.8 Å. Consequently while the $g_{O\text{–}OC}(r)$ and $g_{O\text{–}O}(r)$ suggests there may be intra-molecular hydrogen bonding there is no supporting evidence for this in $g_{O\text{–}H}(r)$ or $g_{OC\text{–}H}(r)$. This finding is in contrast to that of previous molecular dynamics simulations which found some prevalence of glycerol conformations stabilised by intra-molecular hydrogen bonds.[21,23]

Inter-molecular H-Bonding

The inter-molecular RDFs for oxygen- - -hydrogen pair-wise distributions in glycerol are shown in Fig. 6. For inter-molecular bonds (- - -) defines a non-covalent bond and (-) denotes a covalently bound pair. Given our labelling of the glycerol molecules (Fig. 1) there are 4 pair-wise distributions for these atom types, namely $g_{OC\text{-}\,\text{-}\,\text{-}HG}(r)$, $g_{O\text{-}\,\text{-}\,\text{-}HG}(r)$, $g_{OC\text{-}\,\text{-}\,\text{-}H}(r)$ and $g_{O\text{-}\,\text{-}\,\text{-}H}(r)$. For comparison the RDF for pure water at 298 K is shown, labelled $g_{OW\text{-}\,\text{-}\,\text{-}HW}(r)$. This is taken from data which has been previously published.[37] If we first consider the hydroxyl hydrogen (H) and its bond with oxygen we find that both $g_{OC\text{-}\,\text{-}\,\text{-}H}(r)$ and $g_{O\text{-}\,\text{-}\,\text{-}H}(r)$ display a first peak at 1.8 Å. This shows that H has an inter-molecular bond length of 1.8 Å with both the central and distal oxygen atoms in glycerol (red line in Fig. 6). This length is similar to the position of the first peak in $g_{OW\text{-}\,\text{-}\,\text{-}HW}(r)$, and hence the first coordination shell position of water, suggesting that hydroxyl hydrogen atoms (H) in glycerol participate in hydrogen bonding with oxygen atoms (O and OC) in a similar way to that of pure water (HW and OW). In the case of the methyl hydrogen (HG) and its bond with oxygen we find that neither $g_{O\text{-}\,\text{-}\,\text{-}HG}(r)$ and $g_{OC\text{-}\,\text{-}\,\text{-}HG}(r)$ display any prominent peaks. These RDFs suggest that oxygen atoms of glycerol form inter-molecular hydrogen bonds with hydroxyl hydrogen atoms (H) and not with the methyl hydrogen atoms (HG).

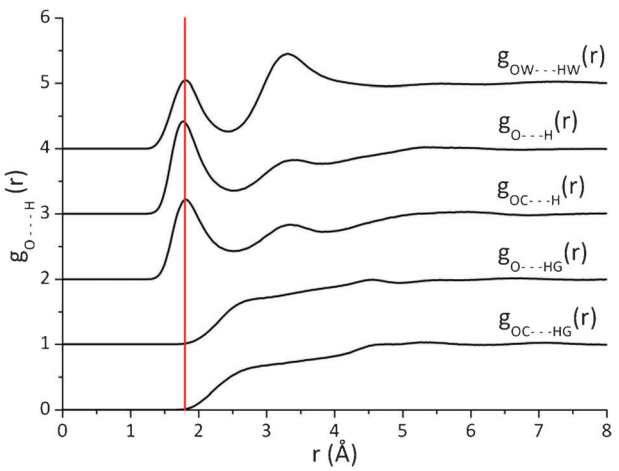

Fig. 6 Partial radial distribution functions (RDFs) for the 4 possible oxygen- - -hydrogen pairings taken from neutron diffraction data and the EPSR simulation of glycerol at 298 K. For comparison the RDF for pure water at 298 K is shown, labelled $g_{OW\text{-}\,\text{-}\,\text{-}HW}(r)$. This is taken from data which has been previously published.[37] A red line at 1.8 Å intersects the first peak of the RDFs of two of the pair-wise distributions for glycerol, namely $g_{O\text{-}\,\text{-}\,\text{-}H}(r)$ and $g_{OC\text{-}\,\text{-}\,\text{-}H}(r)$. It also intersects the first peak of the pure water RDF, $g_{OW\text{-}\,\text{-}\,\text{-}HW}(r)$. This suggests that hydroxyl hydrogen atoms (H) in glycerol participate in hydrogen bonding with oxygen atoms (O and OC) in a similar way to that of pure water (HW and OW). This is not the case for methyl hydrogen atoms in glycerol (HG), which do not show a prominent first peak.

The coordination number for oxygen- - -hydrogen pairings in glycerol have been calculated. This is the average number of atoms of type β that can be found within a defined distance of atoms of type α. This is expressed as,

$$n_{\alpha\beta} = 4\pi\rho c_\beta \int_{r_1}^{r_2} r^2 g_{\alpha\beta}(r)\mathrm{d}r \qquad (5)$$

where c_β is the number fraction of atom β, ρ is the density of the system (atoms Å^{-3}) and $n_{\alpha\beta}$ is the coordination number of β around α. The first minima in the oxygen- - -hydroxyl hydrogen RDFs (Fig. 6) were used as the maximum distance, r_2. This imposes a limit for two atoms to be defined as hydrogen bonded at 2.5 Å. This value is consistent with previous molecular dynamics simulations.[20,21]

The coordination number, using this cut-off shows that there are 0.96 ± 0.61 O- - -H bonds per distal oxygen atom, O, and 0.92 ± 0.63 OC- - H bonds per central oxygen atom, OC, (see Table 8). As there are two distal oxygen atoms and one central oxygen atom per molecule there are 2.84 ± 1.07 oxygen- - -hydrogen bonds per molecule. Therefore, each glycerol molecule donates 2.84 ± 1.07 hydrogen bonds. Our simulation box only contains glycerol; therefore, each molecule must also accept an average of 2.84 ± 1.07 hydrogen bonds. This indicates that there is an average of 5.68 ± 1.51 hydrogen bonds per glycerol molecule (2.84 ± 1.07 as an acceptor and 2.84 ± 1.07 as a donator).

This result is larger than that reported in a number of previous molecular dynamics studies. One such study investigated 32 glycerol molecules treating CH_2 and CH as united 'atoms'[20] and defined a hydrogen bond as having an O- - -H distance below 2.4 Å. This study found a total of 99 inter-molecular and 5 intra-molecular hydrogen bonds within the 32-molecule simulation, resulting in 3.09 inter-molecular and 0.16 intra-molecular hydrogen bonds per molecule. A later study, using the same reference potentials, examined 256 molecules and investigated the effect of pressure on hydrogen bond number.[21] This work defined a hydrogen bond as having an O- - -H distance below 2.4 Å and reported that the number of oxygen- - -hydrogen bonds rose from 1.63 at slightly higher than atmospheric pressure up to 1.84 when pressurised (~0.7 GPa). This equates to an increase from 3.26 to 3.68 hydrogen bonds per molecule. The intra-molecular hydrogen bond number was not shown to be pressure dependant remaining constant at 0.16 bonds per molecule. Both molecular dynamics studies found a much lower number of inter-molecular hydrogen bonds than has been found in the present study.

More recent molecular dynamics simulations examined 1000 glycerol molecules at constant NVT.[23] This work defined a hydrogen bond as having an O- - -H distance below 2.45 Å. The average number of donated hydrogen bonds per molecule was calculated as a function of conformer. The αα conformer at 319.4 K was found to have 1.7 donated hydrogen bonds per molecule indicating 3.4 inter-molecular hydrogen bonds per molecule. Again this number is lower than that reported here.

A recent density functional theory based simulation study was completed using 16 identical glycerol molecules.[38] Here a

Table 8 Coordination numbers for the pair correlations functions represented in Fig. 6 and 7. The standard deviation (σ) has been calculated over 1150 configurations for each of the coordination numbers

Bond	r_1 (Å)	r_2 (Å)	1st peak position (Å)	Coordination number	σ
O–H	0	2.5	1.77	0.96	0.61
OC–H	0	2.5	1.80	0.92	0.63
O–O	2.28	3.39	2.73	1.57	0.87
O–OC	2.28	3.48	2.76	0.84	0.78
OC–OC	2.28	3.51	2.76	0.84	0.80
OC–O	2.28	3.48	2.76	1.69	0.90

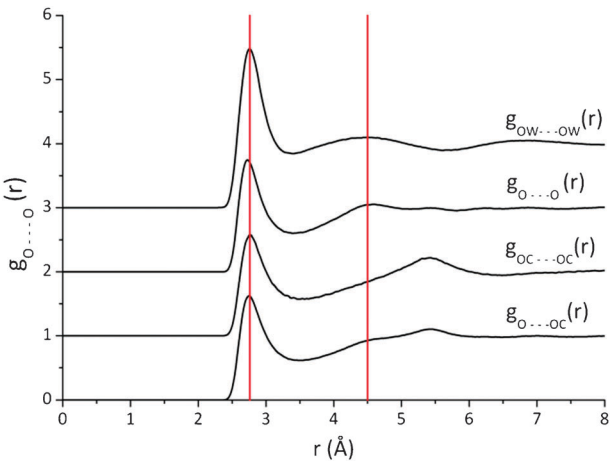

Fig. 7 Partial radial distribution functions (RDFs) for the 3 possible oxygen- - -oxygen pairs ($g_{O\text{-}\text{-}\text{-}O}(r)$, $g_{O\text{-}\text{-}\text{-}OC}(r)$ and $g_{OC\text{-}\text{-}\text{-}OC}(r)$) taken from neutron diffraction data and the EPSR simulation of glycerol at 298 K. For comparison, the RDF for pure water at 298 K is shown, labelled $g_{OW\text{-}\text{-}\text{-}OW}(r)$. This is taken from data which has been previously published.[37] The first and second peaks of the $g_{OW\text{-}OW}$ RDF are shown using red lines. For each glycerol RDF the first peak is at a distance of ~2.8 Å, similar to that of pure water. This distance is consistent with the summation of the inter-molecular distance between oxygen and hydrogen atoms (1.8 Å, Fig. 6) and the intra-molecular distance between oxygen and hydrogen atoms (0.97 Å, Table 2). The second peak in the glycerol RDF differs for each pair-wise distribution; 5.43 Å in $g_{OC\text{–}OC}(r)$, 5.46 Å in $g_{O\text{–}OC}(r)$ and 4.59 Å in intra-molecular. The position of the intra-molecular second peak is similar to that of water, 4.50 Å.

hydrogen bond was defined as having an oxygen- - -oxygen distance of less than 3.5 Å. This lead to an average of 5.7 inter-molecular hydrogen bonds and 0.8 intra-molecular hydrogen bonds per molecule. From Fig. 5 it is clear that using only the oxygen atoms to define a hydrogen bond can lead to an overestimation of the number of bonds that are present. This is because one cannot infer the position of hydrogen atoms to mediate the hydrogen bond from the positions of oxygen atoms. The result for the inter-molecular hydrogen bonds is, nonetheless, much closer to the experimentally derived result in the present study.

X-ray diffraction has also been used to study the hydrogen bonding nature of glycerol.[27] Here the total scattering function is shown to have a prominent peak between 2.8 and 3.0 Å. This peak was attributed to the oxygen- - -oxygen correlation of a hydrogen bond. The signal that would be expected from 6.5 hydrogen bonds with oxygen- - -oxygen length of 2.95 Å was shown to fit this peak closely. The conclusions that could be drawn from this research are limited due to the lack of high Q data and the inability to separate the signals from different atoms unambiguously. This research is, however, in much closer agreement with the results reported here.

Next we consider the oxygen- - -oxygen RDFs in glycerol at 298 K, namely $g_{O\text{-}\text{-}\text{-}O}(r)$, $g_{O\text{-}\text{-}\text{-}OC}(r)$ and $g_{OC\text{-}\text{-}\text{-}OC}(r)$ (Fig. 7). For comparison the RDF for pure water at 298 K is shown, labelled $g_{OW\text{-}\text{-}\text{-}OW}(r)$. This is taken from data which has been previously published.[37] For each glycerol RDF the first peak is at a distance of ~2.8 Å, similar to that of pure water. This distance is consistent with the summation of the inter-molecular distance between oxygen and hydrogen atoms (1.8 Å, Fig. 6) and the intra-molecular distance between oxygen and hydrogen atoms (0.97 Å, Table 2).

The second peak in the glycerol RDF differs for each pair-wise distribution, ranging from 5.46 Å in $g_{O\text{-}\text{-}\text{-}OC}$, to 5.43 Å in $g_{OC\text{-}\text{-}\text{-}OC}$ and 4.59 Å $g_{O\text{-}\text{-}\text{-}O}$, while the second peak in the water RDF $g_{OW\text{-}\text{-}\text{-}OW}$ is at 4.50 Å. This second peak corresponds to the position of the second coordination shell in the system (Fig. 7). Interestingly $g_{OW\text{-}\text{-}\text{-}OW}(r)$ and $g_{O\text{-}\text{-}\text{-}O}(r)$ have a very similar structure. This indicates that the coordination shells of the distal oxygen atoms are very similar to those of water oxygen atoms.

The hydrogen-bonded structure of glycerol has been investigated by measuring the triplet bond angle distributions for oxygen-hydrogen- - -oxygen bonds in the system. Given our labelling of the glycerol molecules (Fig. 1) there are 4 triplet bond angle distributions in this system, namely O–H···O, OC–H···O, O–H···OC and OC–H···OC. Fig. 8 shows the triplet bond angle distribution as a function of angle (θ). In all cases the distribution was calculated over a distance range corresponding to the first peak in the RDF of the oxygen- - -hydroxyl hydrogen function. For comparison the triplet bond angle for pure water at 298 K is shown, labelled OW–HW···OW. From Fig. 8 it is clear that the most probable angle for the triplet of atoms is ~180°, suggesting a planar arrangement of these atoms in the structure of glycerol (see Fig. 8 inset for schematic). This angular distribution is the same as that found in pure water suggesting glycerol adopts a similar hydrogen bonded network to that of water.

To investigate the hydrogen-bonded network further we measured the triplet bond angle distribution for oxygen- - -oxygen- - -oxygen atoms in the system. Fig. 9 shows the triplet bond angle distribution as a function of angle (θ) and shows a broad distribution with a peak at 104.5°. For comparison we show the same distribution for pure water.[37] This data suggests that the oxygen atoms in glycerol are forming a structure which is more disordered than that in pure water (see Fig. 9 inset for schematic).

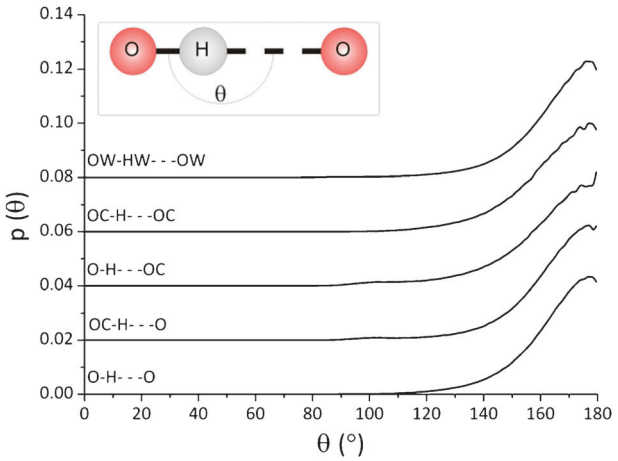

Fig. 8 Triplet bond angle distributions, p(θ), for all possible oxygen-hydrogen- - -oxygen bonds as a function of angle, θ, taken from neutron diffraction data and the EPSR simulation of glycerol at 298 K. For each distribution there is a peak between 175° and 180°. For comparison the RDF for pure water at 298 K is shown, labelled OW-HW- - -OW. This has been taken from previously published data.[37] This suggests that hydrogen bonding between glycerol is close to being linear. Inset: A schematic diagram to show the system that is being studied and the angle, θ.

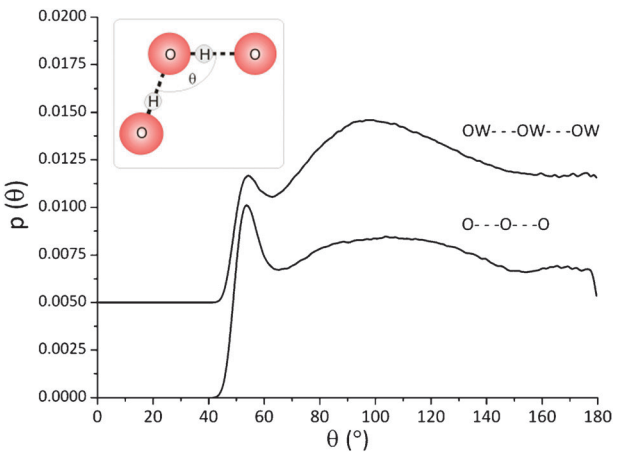

Fig. 9 Triplet bond angle distributions, p(θ), for the combination of the O- - -O- - -O (distal) and OC–OC–OC (central) bonds as a function of angle, θ, taken from neutron diffraction data and the EPSR simulation of glycerol at 298 K. The distribution labelled OW- - -HW- - -OW has been produced using previously published data taken from a neutron diffraction experiment looking at pure water.[37] Inset: A schematic diagram to show the system that is being studied and the angle, θ.

The structure around the carbon atoms has also been investigated. Fig. 10 shows the 3 possible carbon- - -carbon RDFs; CG- - -CG, CG- - -CC and CC- - -CC. The first peak in the CG- - -CG RDF is at 4.44 Å (red line), the CG- - -CC peak is further out at 4.65 Å and the CC- - -CC is further still at 5.16 Å. Therefore, the distal (outer) carbon atoms on separate molecules are closer to each other than the central carbon atoms. For all carbon- - -carbon pair-wise distributions the second coordination shell is at a distance of ~9.45 Å (red line). It can be observed from Fig. 10 that the carbon-carbon

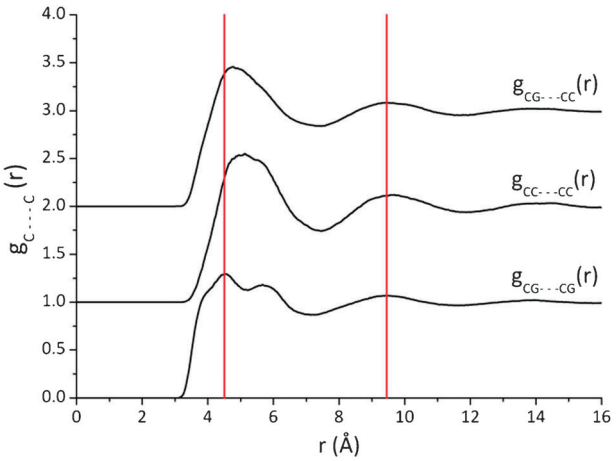

Fig. 10 Partial radial distribution functions (RDF) for the 3 possible carbon- - -carbon pairs taken from neutron diffraction data and the EPSR simulation of glycerol at 298 K. The first peak in the $g_{CG- - -CG}(r)$ RDF is at ~4.5 Å. This peak position increases for the other pair-wise distributions moving out to ~4.8 Å for $g_{CG- - -CC}(r)$ and ~5.1 Å $g_{CC- - -CC}(r)$. The red line at 4.50 Å shows this increase in position. This suggests that the first coordination shell of distal carbon atoms ($g_{CG- - -CG}(r)$) is closer than the first coordination shell of both distal and central carbon atoms ($g_{CG- - -CC}(r)$) and central carbon atoms ($g_{CC- - -CC}(r)$). Interestingly, there is an additional prominent peak in the $g_{CG- - -CG}(r)$ RDFs at 5.67 Å which is not present in the others RDFs. For all RDFs there is a 'second' peak at ~9.5 Å, suggesting the second coordination shell is at a similar distance for all 3 distributions. It is also noteworthy that the carbon- - -carbon RDFs show long-range order up to around 16 Å. This is a greater distance than that of oxygen-oxygen which shows order up to only around 8 Å (see Fig. 7).

RDF has longer-range order (up to around 16 Å) than that of O- - -O (around 8 Å) (see Fig. 7), illustrating longer range order through the methyl group compared with the hydroxyl group.

Conclusions

The aim of this work was to evaluate the conformation and hydrogen bonding properties of pure liquid glycerol. This has been achieved by a combination of neutron diffraction with isotopic substitution and EPSR modelling. This is, as far as the authors are aware, the first experimental determination of the structure of pure liquid glycerol at an atomistic level. The models that have been produced are consistent with the experimental results and provide new insight into the structural properties of an important cryoprotectant molecule. The work has rigorously determined the conformational distribution of glycerol molecules which are consistent with the experimental data. It has shown that there are an average of 5.68 ± 1.51 hydrogen bonds per glycerol molecule and hydrogen bonds between glycerol molecules are approximately linear. Interestingly, the number of inter-molecular hydrogen bonds per molecules is larger than has been reported from earlier molecular dynamics investigations.[20,21,23,24] The hydrogen bond network between glycerol molecules has been investigated and shows a more disordered distribution than pure water. Given that the hydrogen bond lengths and angles are similar to that of water

it is interesting to consider the role played by glycerol in preventing ice formation. We speculate that glycerol and water molecules may mix very effectively hindering the formation of both ice and glycerol crystals. It should be noted that this work forms only the first step in an exhaustive study of the structure of glycerol in various concentrations and at different temperatures.

Acknowledgements

This work was supported by the Engineering Physical Science Research Council, UK through grant EP/H020616 and through a DTA studentship to James Towey. We are grateful to Dr Silvia Imberti and Dr Rowan Hargreaves at the ISIS Facility, Rutherford Appleton Laboratory for their support.

References

1 W. T. Grubbs and R. A. Macphail, *J. Chem. Phys.*, 1994, **100**, 2561–2570.
2 J. Wuttke, J. Hernandez, G. Li, G. Coddens, H. Z. Cummins, F. Fujara, W. Petry and H. Sillescu, *Phys. Rev. Lett.*, 1994, **72**, 3052–3055.
3 L. Dougan, G. Fang, H. Lu and J. M. Fernandez, *Proc. Natl. Acad. Sci. U. S. A.*, 2008, **105**, 3185–3190.
4 K. Gekko and S. N. Timasheff, *Biochemistry*, 1981, **20**, 4667–4676.
5 P. H. Yancey, M. E. Clark, S. C. Hand, R. D. Bowlus and G. N. Somero, *Science*, 1982, **217**, 1214–1222.
6 J. L. Dashnau, N. V. Nucci, K. A. Sharp and J. M. Vanderkooi, *J. Phys. Chem. B*, 2006, **110**, 13670–13677.
7 C. Polge, A. U. Smith and A. S. Parkes, *Nature*, 1949, **164**, 666–666.
8 S. Mironesc, T. Seed and H. Meryman, *Journal of Cell Biology*, 1974, **63**, A229–A229.
9 C. S. Callam, S. J. Singer, T. L. Lowary and C. M. Hadad, *J. Am. Chem. Soc.*, 2001, **123**, 11743–11754.
10 E. C. H. To, J. V. Davies, M. Tucker, P. Westh, C. Trandum, K. S. H. Suh and Y. Koga, *J. Solution Chem.*, 1999, **28**, 1137–1157.
11 A. Doss, M. Paluch, H. Sillescu and G. Hinze, *J. Chem. Phys.*, 2002, **117**, 6582–6589.
12 J. M. Vanderkooi, J. L. Dashnau and B. Zelent, *Biochim. Biophys. Acta, Proteins Proteomics*, 2005, **1749**, 214–233.
13 A. Doss, M. Paluch, H. Sillescu and G. Hinze, *Phys. Rev. Lett.*, 2002, **88**, 095701–095705.
14 R. L. Cook, H. E. King, C. A. Herbst and D. R. Herschbach, *J. Chem. Phys.*, 1994, **100**, 5178–5189.
15 D. B. Davies, A. J. Matheson and G. M. Glover, *J. Chem. Soc., Faraday Trans. 2*, 1973, **69**, 305–314.
16 D. C. Champeney and F. O. Kaddour, *Mol. Phys.*, 1984, **52**, 509–523.
17 N. Menon and S. R. Nagel, *Phys. Rev. Lett.*, 1995, **74**, 1230–1233.
18 R. Bohmer and G. Hinze, *J. Chem. Phys.*, 1998, **109**, 241–248.
19 O. Bastiansen, *Acta Chem. Scand.*, 1949, **3**, 415–421.
20 L. J. Root and F. H. Stillinger, *J. Chem. Phys.*, 1989, **90**, 1200–1208.
21 L. J. Root and B. J. Berne, *J. Chem. Phys.*, 1997, **107**, 4350–4357.
22 R. Chelli, F. L. Gervasio, C. Gellini, P. Procacci, G. Cardini and V. Schettino, *J. Phys. Chem. A*, 2000, **104**, 5351–5357.
23 R. Chelli, P. Procacci, G. Cardini and S. Califano, *Phys. Chem. Chem. Phys.*, 1999, **1**, 879–885.
24 R. Chelli, P. Procacci, G. Cardini, R. G. Della Valle and S. Califano, *Phys. Chem. Chem. Phys.*, 1999, **1**, 871–877.
25 M. Garawi, J. C. Dore and D. C. Champeney, *Mol. Phys.*, 1987, **62**, 475–487.
26 D. C. Champeney, R. N. Joarder and J. C. Dore, *Mol. Phys.*, 1986, **58**, 337–347.
27 S. Sarkar and R. N. Joarder, *Phys. Lett. A*, 1996, **222**, 195–198.
28 H. E. Fisher, A. C. Barnes and P. S. Salmon, *Rep. Prog. Phys.*, 2006, **69**, 233–299.
29 D. A. Keen, *J. Appl. Crystallogr.*, 2001, **34**, 172–177.
30 A. K. Soper, S. Howells and A. C. Hannon, *Technical Report*, RAL-89-046 Rutherford Appleton Laboratories, Oxon, UK, 1999.
31 A. K. Soper, *Mol. Phys.*, 2009, **107**, 1667–1684.
32 A. K. Soper, *Phys. Rev. B: Condens. Matter Mater. Phys.*, 2005, **72**, 104204–104211.
33 G. Hummer, D. M. Soumpasis and M. Neumann, *J. Phys.: Condens. Matter*, 1994, **6**, A141–A144.
34 A. K. Soper, *Chem. Phys.*, 1996, **202**, 295–306.
35 H. van Koningsveld, *Recl. Trav. Chim. Pays-Bas*, 1968, **87**, 243–249.
36 J. Dawidowski, F. J. Bermejo, R. Fayos, R. F. Perea, S. M. Bennington and A. Criado, *Phys. Rev. E: Stat. Phys., Plasmas, Fluids, Relat. Interdiscip. Top.*, 1996, **53**, 5079–5088.
37 A. K. Soper, *J. Phys.: Condens. Matter*, 2007, **19**, 335206–335224.
38 W. Zhuang and C. Dellago, *J. Phys. Chem. B*, 2004, **108**, 19647–19656.
39 T. Hassinen and M. Perakyla, *J. Comput. Chem.*, 2001, **22**, 1229–1242.

